HiSST: 2nd International Conference on
High-Speed Vehicle Science Technology
11–15 September 2022, Bruges, Belgium

Numerical investigation of leading-edge bluntness effect on Scramjet inlet at Mach 6

Talluri Vamsi Krishna[1], Saranyamol VS[1], Desikan SLN[2], Mohammed Ibrahim Sugarno[1]

Abstract

The leading-edge bluntness plays an important parameter in influencing separation and shock boundary layer interactions. Current work is to investigate the effect of the sharp and blunt leading edges at Mach 6 to understand the wall heat fluxes and flow characteristics of a scramjet intake. A detailed two -dimensional computational study carried out using commercially available Ansys Fluent software. Three different nose tip radii of 0, 0.5 & 1.0 mm analyzed for ramp and cowl individually. Radius of 0.5 mm shows no significant change in the flow field for the all the configurations simulated. When the tip radius increased to 1.0 mm, peak pressure loads were increased marginally and peak heat transfer to the wall decreased significantly for all the configurations tested. This study provided better insights into understanding nose tip bluntness effect on ramp, cowl and combination of both with respect to shock boundary layer intractions.

Keywords : *Scramjet, Inlet, SWBLI, Separation bubble, Boundary layer*

1. Introduction

The objective of the Intake is to provide a consistent air supply into the combustion chamber with the lowest possible total pressure loss and high compression ratio. Intake will generally have a sharp leading edge to reduce the total pressure loss or minimize the drag by creating a weak oblique shock. However, sharp leading edges are prone to extreme aerodynamic heating [1]. To overcome extreme heating, modifications to the leading edge has proposed, and this will completely change the flow field inside the Inlet. Shock wave boundary layer interactions (SWBLI) play an essential role in the scramjet inlet performance, and they may significantly change the flow field structure [2–5]. The growth of the boundary layer thickness at the leading edge in hypersonic speeds is higher than at supersonic speeds. When the blunt leading edge replaces a sharp leading, it produces an induced pressure gradient and reduced boundary layer thickness. Nevertheless, this thinning of boundary layer thickness has higher kinematic viscosities, surface temperatures and higher skin friction coefficient. Thus, the leading-edge bluntness influences the flow inside the Inlet and should be treated as an essential parameter while designing the Inlet [6]. When a shock wave interacts with this boundary layer leads to flow separation and increases wall heat flux, and induced pressure at the reattachment point. These effects will significantly reduce the inlet efficiency and adversely affect the isolator's flow properties, leading to an Inlet unstart [7]. SWBLIs and shock-shock interaction regions are potential zones for localized elevated heating rates [8–12] in the inlet region. The study on effect of leading-edge bluntness over wedges, cones and ramps carried out by many researchers over last few decades. Holden [13,14] has studied effect of leading-edge bluntness in ramps with the help of theoretical analysis and experimental investigation. In this work it was observed that the separation region length increases until it reaches the critical radius of the leading edge. Then separation region length decreases with further increase of radius at hypersonic Mach number. Neuenhahn and Olivier [15] studied the effect of leading-edge bluntness over double wedge at hypersonic flows, they did not observe any separation length reversal after the critical radii. Kim et al. [16] conducted an experimental study over double wedge with effect

[1] Post *Graduate student, Indian Institute of technology Kanpur, India (sri.vamsi1432@gmail.com)*
[2] Post *Graduate student, Indian Institute of technology Kanpur, India (saranya@iitkac.in)*
[3] *Senior scientist, Vikram Sarabhai Space Centre, ISRO, Thiruvananthapuram, India (desikan_sln@yahoo.com)*
[4] Assistant Professor, Indian Institute of technology Kanpur, India (Ibrahim@iitk.ac.in)

of nose tip bluntness at Mach 4. In this study nose tip radius varied from the 0 to 2mm, they observed small change in the bluntness radius changes flow features significantly. The separation location moved to upstream when they increased the bluntness up to 1.0 mm and further increase in bluntness radius did not affect flow features notably.

Despite many efforts by researchers, there is still room for a better understanding of the separation bubble dynamics, ~~and~~ shock infractions that causes the Intake to unstart and higher wall heat transfers due to separation. The present work aims to study scramjet inlets at Mach 6 with sharp and blunt leading-edges numerically, and its effect on separation region dynamics; pressure distribution, wall heat flux etc.

2. Numerical setup

Simulations are performed using the ANSYS Fluent 18.1, and mesh is generated using the Ansys workbench. For time independent simulations, a steady-state Reynolds Averaged Numerical simulation (RANS) is carried out. An implicit density-based double-precision flow solver is used to solve conservation equations. The turbulence model of k-ε RNG is selected for current simulations along with the Advection Upstream Splitting Method (AUSM) to calculate the convective flux vector. A spatial discretization scheme based on the green gauss node-based approach is adopted, with second-order upwind for spatial accuracy. Air is considered as a thermally perfect gas, and viscosity is calculated based on three equations of Sutherland's law. The simulations are carried out until convergence is obtained up to a minimum of 10^{-5}.

3. Model Details:

The current scramjet inlet consists of external compression ramps with 10.5° and 21° and expansion ramps to turn the incoming flow back into the intake. The isolator has a height (h) of 15 mm and a width (W) of 120 mm. The cowl is having compression of 6.0. The fig.1 shows a schematic of the intake used for the present simulations along with the computational domain and associated boundary conditions. Three different nose tip radii of 0, 0.5 & 1 mm with four different combinations for ramp and cowl viz. both ramp and cowl as sharp, only ramp nose tip blunted, only cowl nose tip blunted and both tips blunted.

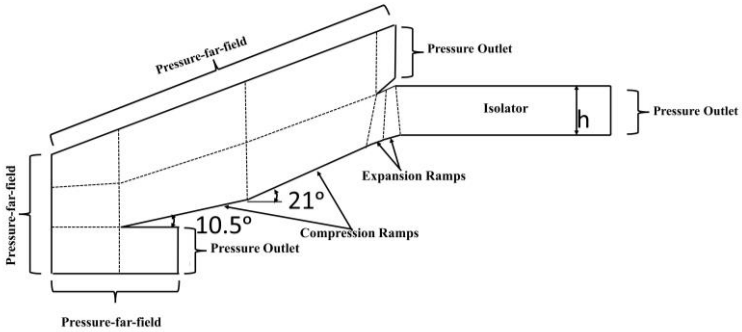

Fig 1. Schematic diagram of Intake with computational domain

Table 1. Flow conditions used for the present numerical simulations

Test conditions	
Total Enthalpy H_0(MJ.kg^{-1})	0.9
Free stream Pressure p_∞ (Pa)	318.3
Free Stream Temperature T_∞(°K)	110.5
Free stream Mach Number M_∞	6
Free stream velocity u_∞ (ms^{-1})	1264

4. Results

Present numerical simulations are carried out to study the effect of nose tip bluntness on scramjet ramp and cowl. The simulations were carried out at Mach 6 flow with free steam total enthalpy of 0.9 MJ/kg, corresponding to the S1 tunnel condition. The test conditions used for the current simulations are presented in Table 1.

Validation and Grid Independence

To verify the independence of the flow solution with respect to the present computational mesh size, grid independency analysis is carried out. Three different gird sizes used for the current setup, small (Mesh 1) consists of 0.3 million nodes, medium (Mesh 2) has 0.42 million and large Mesh has 0.6 million nodes. Figure 2 shows the normalized pressure along the cowl length obtained with all the grids in comparison to the experimental results obtained by Le et al. [17]. Irrespective of the grid size, the computational result is seen to have good agreement with the experimental results [17]. For better postprocessing of numerical schlieren imaging larger grid with 0.6 million nodes is used for the simulations.

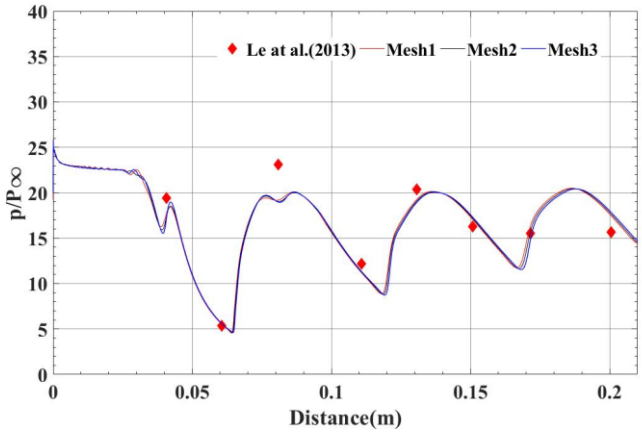

Fig 2. Plot showing the experimental [17] and computed wall-static pressure (Grid-1, Grid-2, Grid-3) on the cowl surface of the intake

All the numerical simulations carried out in steady state at Mach 6, and Fig. 3 shows the computed normalized pressure and wall heat flux for a sharp nose tip. When the incoming flow interact with the first compression ramp (10.5°) creates an oblique shock resulting in the normalized pressure ratio increment to 4.0 and this increment is well matched with the theoretical value of 3.9 from oblique shock relations. It stays constant up to x location of 104 mm, where the first ramp ends, and second compression ramp begins. Because of this second compression ramp (21°), another oblique shock is formed and creates a sudden jump in the pressure ratio to 11.6. From the oblique shock relations, theoretical pressure ratio for 2nd compression ramp is calculated to be 11.9. On both ramps, a minor change in the pressure ratio is noticed and it may be due to the viscous model used in the simulations. This jump in pressure ratio is constant throughout the 2nd ramp (up to 174 mm) and then pressure suddenly drops due to 1st expansion ramp; expansion happens up to end of the 1st expansion ramp. On the initial section of second ramp, we can observe the expansion flow, but separation bubble is catching up to the 2nd expansion ramp and thereby nullifying the use of 2nd expansion ramp. On the 2nd expansion ramp due to separation shock, pressure start to rise and stay constant in separation region and then sudden rise in pressure observed due to the reattachment shock and reaches the peak at reattachment point. Then pressure decreases due to flow expansion in the isolator and then increases due to refection shock from the cowl side. Wall heat transfer shown the fig.3(b) follows similar trend as pressure on ramp surface. Heat transfer peak is observed at shock reattachment point and peak heat transfer for this case is found to be 27 W/cm$^{2.}$ Figure 4 show the numerical schlieren and vorticity contours along with streamlines overlapped within it for the sharp nose tip configuration. Numerical schlieren shows(fig.4a), when the cowl shock interacts with the boundary layer on the ramp creates an

adverse pressure gradient and it leads to boundary layer to separation. The reattachment shock and reflection shock from cowl is clearly visible. From fig.4(b), separation region is visible with separation bubble spanning up to the 2nd expansion ramp.

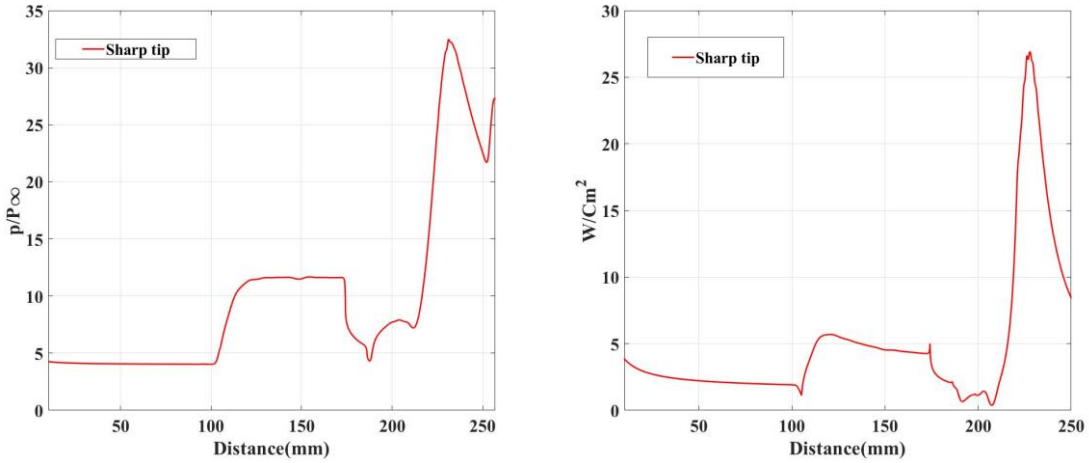

(a) Normalized Pressure distribution (b) Wall heat transfer

Fig 3. Normalized pressure and wall heat flux distribution along the ramp to isolator for sharp tip at Mach 6

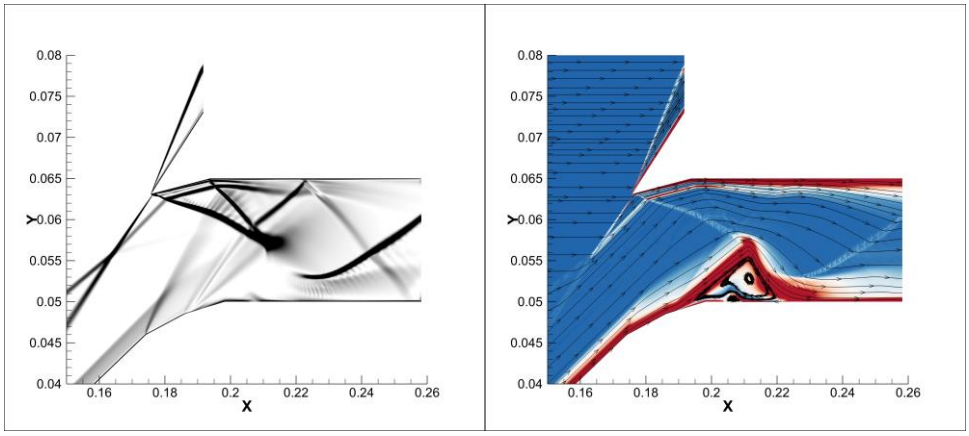

(a)Numerical Schlieren (b) Vorticity Contour

Fig 4. Numerical schlieren and vorticity contour for sharp tip configuration

The comparison of normalized pressure and wall heat flux for blunt configurations with nose tip radius of 0.5 mm shown in the fig.5. This nose tip bluntness tested for both ramp and cowl individually to see the effect of bluntness on ramp as well as cowl. Figure 5 (a) shows the normalized pressure along ramp and isolator with bluntness radius of 0.5 mm and these results were compared to the sharp nose tip. There is no significant change in pressure variation along ramp and isolator except the reattachment location and the pressure rise at the 2nd ramp starting. For ramp tip and both tips blunted configuration, pressure rise on the 2nd ramp is not a steep rise as sharp tip due to formation of High entropy layers. Due to blunt nose tip radius, the bow shock is formed instead of the oblique shock entropy gradient created is created normal to flow direction. The entropy gradients will form a strong vortical activity just above the boundary layer and produces a stabilizing effect which counters the destabilizing effect of reduced Mach number due stronger bow shock [18]. The peak pressure load is occurring inside the isolator for the all configurations and is highest for the blunted cowl tip configuration and lowest for the blunted ramp tip configuration with 5% decrement, as compared to the sharp tip. The separation region length appears to be same for the all the configurations.

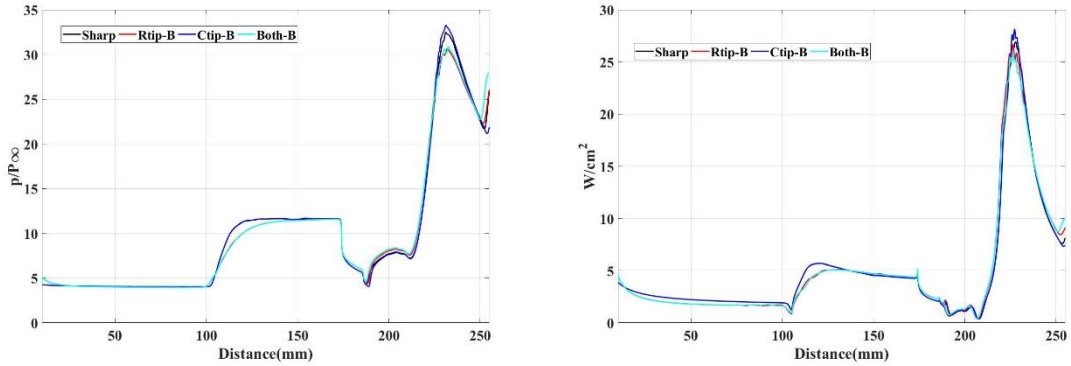

(a) Normalized pressure (b) Wall heat transfer

Fig 5. Normalized pressure and total wall heat transfer along the ramp and isolator for modified nose tip bluntness of 0.5 mm

Fig. 5(b) shows the wall heat transfer along the ramp and isolator. All the configurations show the similar trend in the wall heat transfer. The reduction in the peak heat transfer rates were for the ramp tip and both tips blunted configurations. The reduction in wall heat transfers compared to sharp tip configuration were 1 & 3.5% for ramp tip and both tips blunted configurations respectively. Whereas the cowl tip blunted configuration showed 4.5% increase the wall heat transfer rate compared to the sharp tip configuration. Numerical schlieren flow visualization and vorticity contours for the without and with nose tip bluntness configurations were shown in fig.6. Numerical schlieren suggests, no significant change in the flow field due to the nose tip bluntness of radius 0.5 mm. Entropy layer on the cowl inner wall can be seen in the cowl tip bluntness and both tips blunted configurations. The fig.6 (II) shows the vorticity contours along with streamlines overlapped over it for without and with blunted nose tip configurations. The vorticity contours also suggest flow field inside the isolator looks similar to the sharp case and there was no significant change in shock boundary layer interactions due the nose tip bluntness of 0.5mm.

(I)

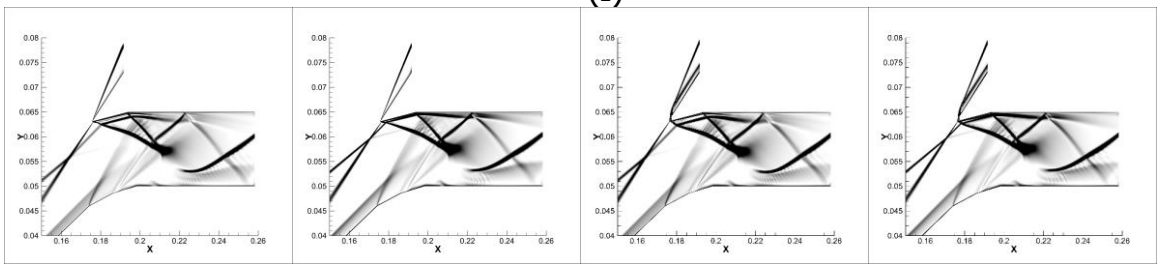

(a)Sharp Tip (b) R-tip bluntness (c) C-tip bluntness (d) Both

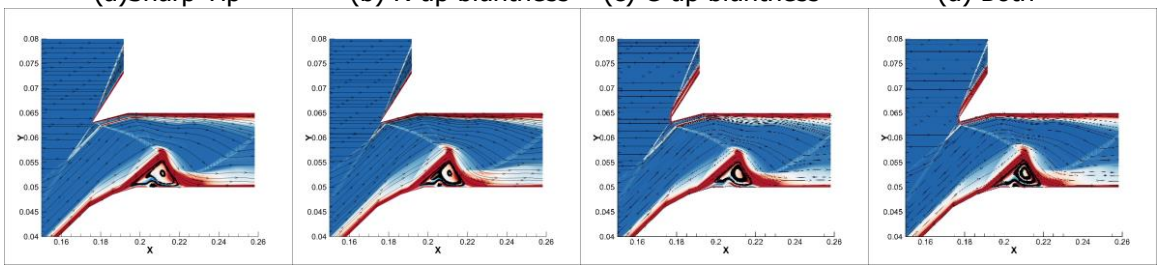

(II)

Fig 6. Comparison of numerical schlieren(I) and vorticity contours (II) of with and without nose tip bluntness for radius of 0.5 mm.

Normalized pressure and wall heat transfer along the ramp and isolator of without and with nose tip bluntness with radius of 1.0 mm shown in the fig.7. The blunted cowl nose tip configuration shows similar trend in pressure variation, minor change in the separation pressure noticed. The reflected pressure appeared to be stronger than the sharp nose tip due to stronger separation shock. For the ramp tip and both tips bunted configurations pressure ratio decrement seen at the 2nd ramp starting. Peak pressure load and separation pressure ratios were observed highest for both nose tips blunted configuration. Reattachment pressure has decreased compared to the sharp nose tip, but reflected

shock became strong and peak pressure load is occurring at the impinging point of reflected shock. For nose tip bluntness of 1 mm radius, increment in the pressure load observed for all the configurations and highest increment in the pressure observed when both tip radius were blunted. When both nose tips are blunted, 16% increment in pressure observed as compared to sharp tip configuration. Figure 7(b) shows the wall heat transfer along the ramp and isolator region for nose tip radius of 1 mm. Wall heat transfer data shows, blunted cowl tip and sharp tip shows similar trend and slight decrement in peak heat transfer rate observed. Modified ramp tip and both nose tips blunted configurations show decrement in the heat transfer at 2nd ramp starting and heat transfer increases gradually compared to sharp tip configuration, where heat transfer increment is sudden. Decrement in peak heat transfer observed for the all the configurations and highest reduction observed of when only ramp nose tip is blunted followed by only cowl tip is blunted. Pressure and heat transfer data suggests separation pressure increase in order of blunted cowl, then ramp tip followed by both nose tips blunted. Separation shock angle also increases in the same order and reflected shock impingements moves in upstream direction with higher shock strength.

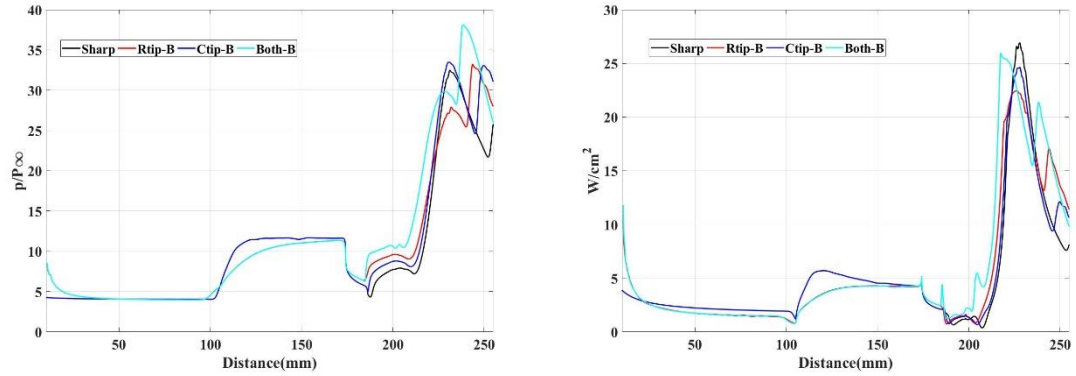

(a) Normalized pressure (b) Wall heat transfer

Fig 7. Normalized pressure and total wall heat transfer along the ramp and isolator for modified nose tip bluntness of 1.0 mm

(I)

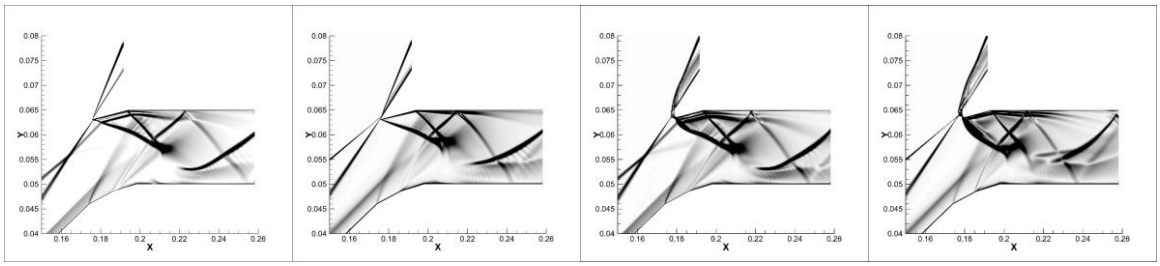

(a)Sharp Tip (b) R-tip bluntness (c) C-tip bluntness (d) Both

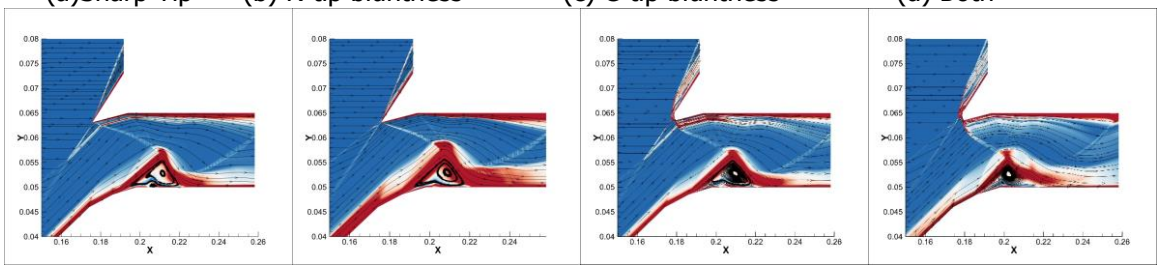

(II)

Fig 8. Numerical Schlieren(I) and vorticity contours (II) without and with nose tip bluntness for radius of 1.0 mm

Numerical schlieren and vorticity contours for blunted nose tip radius of 1.0mm presented in fig.8. From the numerical schlieren(fig.8(I)), shock wave formation due to cowl and ramp tips, interactions of cowl shock with boundary layer, reflected shock from the cowl surface and separation region flow pattern is clearly observed. When the nose tip blunted with 1.0 mm, both ramp and cowl shocks become curved,

shock strength becomes higher, as well as they create a high entropy region larger than 0.5 mm with higher pressure gradients. These high-pressure gradient zones impacted by high strengths shock waves leads to stronger separation. From numerical schlieren, it was observed reflected shock moved towards upstream as bluntness changed in order of cowl, ramp, both nose tips blunted. This was also correlated with pressure plot from the fig.7(a). The vorticity contours for the blunted nose tip radius of 1.0mm shown in the fig.8 (II). Vorticity contours suggests minor change in the separation region length and incoming entropy layer thickness for without and with nose tip bluntness.

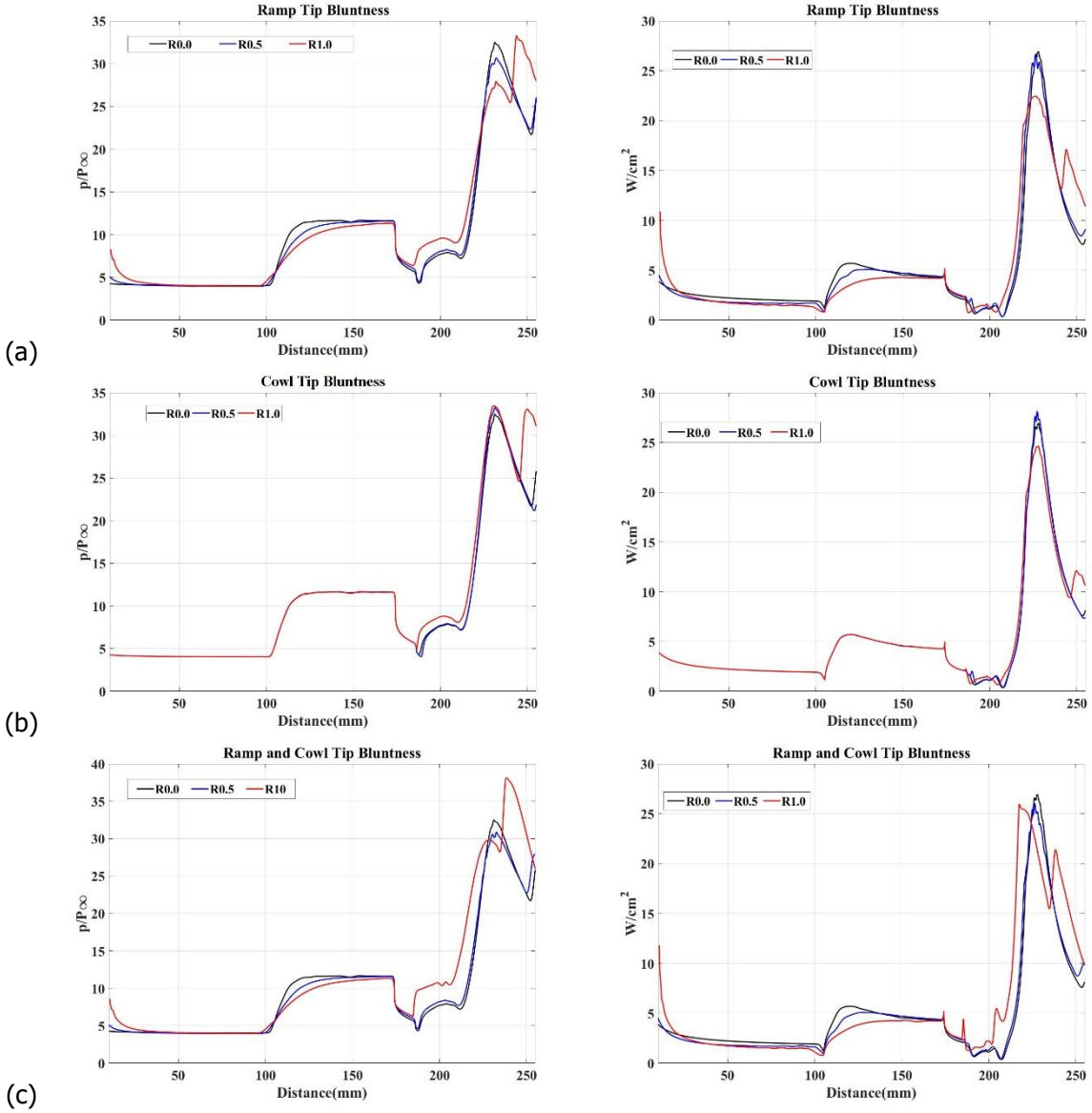

Fig 9. Comparison of normalized surface pressure and wall heat flux for nose tip bluntness with radius of 0, 0.5, 1.0mm.
(a) Ramp tip bluntness (b) Ramp tip bluntness (c) Both

Figure 9 (a) shows comparison of surface pressures and wall heat transfer for the ramp nose tip radius of 0, 0.5, 1.0mm. When the ramp nose tip radius is increased from 0 to 1.0mm, pressure on 2nd compression ramp started decreasing and separation pressure is increasing. Peak pressure load decreased for 0.5 mm and increased for the 1.0mm. Whereas peak heat transfer decreased for both configurations and with a highest decrement of 16% observed for the ramp tip radius of 1.0mm. For the cowl tip modification, computed pressure and heat transfer measurements shown in the fig.9(b). For both configurations, marginal increase in the peak pressure load observed. Heat transfer data showed mixed result, for nose tip radius of 0.5 mm increment in the heat transfer was observed and for the tip radius of 1.0 mm, peak heat transfer was decreased (8.8%). Table 2 shows the computed peak pressure ratio, peak wall heat transfer, percentage change in the peak heat transfer and

normalized pressure with respect to the sharp leading edge. Figure 9(c) shows the pressure and heat transfer plots when both nose tips were blunted modified from 0 to 1.0 mm. As both nose tips changed to tip radius of 0.5 mm, reduction in both pressure and heat loads is observed. However, for nose tip radius of 1.0mm, pressure load increased significantly (17 %) and heat transfer decreased marginally.

Table 2. Computed peak pressure and heat transfer for the without and with nose tip bluntness

S. No.	Configuration	p/P∞	% Change w.r.t Sharp tip	HF(W/cm2)	% Change w.r.t Sharp tip
1	Sharp	32.48	NA	26.93	NA
2	Rtip-0.5 mm	30.67	-5.57	26.64	-1.08
3	Rtip-1.0 mm	33.27	2.43	22.45	-16.63
4	Ctip-0.5mm	33.29	2.50	28.17	4.60
5	Ctip-1.0mm	33.48	3.08	24.55	-8.84
6	Both-0.5mm	30.89	-4.90	26.02	-3.38
7	Both-1.0mm	38.13	17.40	25.97	-3.56

5. Conclusions

The effect of leading-edge nose tip bluntness in scramjet intake at Mach 6 investigated numerically by commercially available Ansys fluent software. To understand the effect of bluntness on shock boundary layer interactions, nose tip radius varied from 0 to 1mm. The effect of nose tip bluntness studied individually on ramp, cowl and combination of both. A steady RANS based numerical scheme is successfully validated for the hypersonic flow and results are well matched with the experiments from the literature. Present study suggests, when the 0.5 mm radius is used, no significant change in the flow field is observed for the all the configurations. The decrement in the peak pressure loads and heat transfer loads compared sharp nose tip configuration observed for the ramp tip and both tips blunted configurations. Whereas, as the nose tip radius increased to 1.0mm, flow field dynamics changes significantly due to high strength curved shocks. For all the configurations, increment in the pressure loads are observed and highest increment is seen for both nose tips blunted to 1.0mm. But peak heat transfer is decreased for the all the configurations and highest decrement observed when only ramp tip is blunted. This study provides the better understanding of the nose tip bluntness parameter on shock boundary layer interactions on the ramp and cowl separately.

Acknowledgments

This work was supported by STC Cell of IITK having grant Number STC/AE/2020196. This work carried out in Department of Aerospace Engineering at Indian Institute of Technology Kanpur, India. All the numerical simulations carried out in High Performance Computing Facility available at CC, IIT Kanpur.

Reference

1. Kasen, S. D. Thermal Management at Hypersonic Leading Edges, Ph.D. dissertation, University of Virginia, Charlottesville, VA, (2013).
2. Anderson JD Jr, Hypersonic and high temperature gas, McGraw-Hill Book, New York, p 690, (1980)
3. Redford, J.A., Sandham, N.D., and Roberts G.T., Numerical simulations of turbulent spots in supersonic boundary layers: effects of Mach number and wall temperature. Prog. Aerosp. Sci. (2011)
4. Krishnan, L., and Sandham, ND., Strong interaction of a turbulent spot with a shock-induced separation bubble., Phys. Fluids., 19, 016102, (2007)
5. Krishnan, L., Sandham N.D., and Steelant, J., Shock-wave/boundary-layer interactions in a model scramjet intake., AIAA J, 47(7), 1680–1691(2009)
6. Kendall, J.M.J. An experimental investigation of leading-edge shock-wave–boundary-layer interaction at Mach 5.8., J. Aeronaut. Sci. 24, 47–56.(1957)
7. Reinartz, B., Ballmann J., and Boyce, R. Numerical investigation of wall temperature and entropy layer effects on double wedge shock/boundary layer interactions., In: AIAA/AHI space planes and hypersonic systems and technologies conference, AIAA , 14 Washington, DC, pp 1–11

8. Grasso, F., and Marini, M., Analysis of Hypersonic Shock-Wave Laminar Boundary-Layer Interaction Phenomena, Comput. Fluids, 25(6), 561–581 (1996).
9. John, B., Vinayak, N. K., and Ganesh, N., Shock Wave Boundary Layer Interactions in Hypersonic Flows, Int. J. Heat Mass Transfer, 70, 81–90 (2014).
10. John, B., and Kulkarni, V., Effect of Leading-Edge Bluntness on the Interaction of Ramp Induced Shock Wave with Laminar Boundary Layer at Hypersonic Speed., Comput. Fluids, 96,177–190 (2014).
11. Savino, R., and Paterna, D., Blunted Cone-Flare in Hypersonic Flow, Comput. Fluids, 34(7), 859–875 (2005).
12. Marini, M. Analysis of Hypersonic Compression Ramp Laminar Flows Under Sharp Leading-Edge Conditions, Aerosp. Sci. Technol., 5(4), 257–271(2001).
13. Holden,M.S., Boundary-layer displacement and leading edge bluntness effects on attached and separated laminar boundary layers in a compression corner. PartI: Theoretical study, AIAA J., 8 (12), 2179-2188(1970).
14. Holden, M.S., Boundary-layer displacement and leading edge bluntness effects on attached and separated laminar boundary layers in a compression corner. PartII: Experimental study, AIAA J., 9 (1), 84-93(1971).
15. Neuenhahn, T., and Olivier, H., Influence of the wall temperature and the entropy layer effects on double wedge shock boundary layer interactions, AIAA J., 2006-8136 (2006).
16. Kim, I., Park, G., and Byun, Y.H., Experimental investigation of the effects of leading-edge bluntness on supersonic flow over a double compression ramp, J. Mecha. Sci. and Tech., 34 (10), 4193-4199(2020).
17. Li, Z., Gao,W., Jiang, H., and Yang, J., Unsteady behaviors of a hypersonic inlet caused by throttling in shock tunnel, AIAA J., 51, 2485–2492 (2013).
18. John, B., Kulkarni, V.N., and Natarajan, G., Shock wave boundary layer interactions in hypersonic flows, International Journal of Heat and Mass Transfer, 70, 81–90 (2014).